Decoding the rules of recruitment of excitatory interneurons in the adult zebrafish locomotor network

Jessica Ausborn, Riyadh Mahmood, and Abdeljabbar El Manira[1]

Department of Neuroscience, Karolinska Institute, 171 77 Stockholm, Sweden

Edited by Eve Marder, Brandeis University, Waltham, MA, and approved November 19, 2012 (received for review September 18, 2012)

Neural networks in the spinal cord transform signals from the brain into coordinated locomotor movements. An optimal adjustment of the speed of locomotion entails a precise order of recruitment of interneurons underlying excitation within these networks. However, the mechanisms encoding the recruitment threshold of excitatory interneurons have remained unclear. Here we show, using a juvenile/adult zebrafish preparation, that excitatory V2a interneurons are incrementally recruited with increased swimming frequency. The order of recruitment is not imprinted by the topography or the input resistance of the V2a interneurons. Rather, it is determined by scaling the effect of excitatory synaptic currents by the input resistance. We also show that the locomotor networks are composed of multiple microcircuits encompassing subsets of V2a interneurons and motoneurons that are recruited in a continuum with increased swimming speeds. Thus, our results provide insights into the organization and mechanisms determining the recruitment of spinal microcircuits to ensure optimal execution of locomotor movements.

central pattern generator | synaptic transmission | Chx10

Neural networks in the spinal cord generate locomotion and serve in a variety of behavioral contexts (1–7). They undergo continuous adjustments to accommodate the contextual demands to produce locomotor movements with appropriate speed, force, and timing. An appreciable understanding of the molecular logic of the assembly of spinal circuits at early developmental stages has begun to emerge (8–21). However, the mechanisms underlying speed control of locomotor movements have remained unclear.

Changing locomotor speed ultimately involves a sequential activation of different motoneurons that represent the final stage of processing in the spinal cord (22–24). However, motoneurons are not primarily involved in the generation of the locomotor rhythm, a task undertaken by premotor interneurons. V2a interneurons are a neuronal class of critical importance to the vertebrate locomotor network (1, 8, 12, 15, 25–35). Partial ablation of these interneurons in zebrafish decreases the excitability of the spinal networks (30). Thus, changes in the speed of locomotor movements would be initiated at the level of V2a interneurons that set the excitatory tone within the locomotor networks. The pattern of activation of V2a interneurons during locomotion has been examined in zebrafish larvae and embryos and in newborn mice (15, 32, 36). However, the mechanisms defining the recruitment threshold of V2a interneurons as a function of locomotor frequency have remained obscure.

We have investigated how V2a interneurons are recruited at different swimming speeds in the juvenile/adult zebrafish. Our findings show that although the excitatory drive of V2a interneurons is graded topographically, their order of recruitment does not obey a topographic map. Rather their recruitment threshold is set by a scaling of the excitatory drive by the input resistance that results in a nontopographic incremental recruitment of V2a interneurons to cover the full range of swimming frequencies. Finally, the existence of a tight temporal relationship between V2a interneuron and motoneuron synaptic inputs suggests that the locomotor networks are composed of a set of overlapping microcircuits. Deciphering the organizational logic of spinal interneurons is essential to further our understanding of how locomotor patterns are generated and, more generally, of how neural microcircuits with distinct organizational schemes interact to generate appropriate outputs.

Results

Activity Pattern of V2a Interneurons at Different Swimming Frequencies. We previously have shown that motoneurons in juvenile/adult zebrafish are organized into four pools that are recruited incrementally in a topographic order to produce swimming at different speeds (22). We therefore sought to determine if the pattern of recruitment of V2a interneurons complies with the topographic and mechanistic principles seen in motoneurons. We used a transgenic zebrafish line in which GFP expression is driven by the promoter of the transcription factor Chx10, which characterizes V2a interneurons (Fig. 1*A*) (15). Swimming activity was induced by electrical stimulation of descending axons in an in vitro brainstem-spinal cord preparation and was monitored by recording from a peripheral motor nerve (Fig. 1*B*) (37). V2a interneurons were recorded at different dorsoventral and lateromedial positions using patch-clamp techniques (Fig. 1 *B*–*D*).

Activity patterns of V2a interneurons during swimming episodes varied considerably among neurons. Some V2a interneurons were not recruited, received only subthreshold synaptic inputs, and never fired a single action potential (Fig. 2*A*), whereas others were recruited in at least one locomotor cycle during which they fired one or multiple action potentials (Fig. 2 *B* and *C*). The peak-to-trough amplitude of locomotor-related synaptic membrane potential oscillations in nonrecruited V2a interneurons was relatively low (2.9 ± 0.3 mV at 4–5 Hz swimming frequency; $n = 22$; Fig. 2*A*). The recruited interneurons displayed larger locomotor-related membrane potential oscillations (14.1 ± 0.8 mV at 4–5 Hz swimming frequency; $n = 26$; Fig. 2 *B* and *C*) and also showed differences in their firing patterns. Some V2a interneurons were transiently recruited (Fig. 2*B*), whereas others were recruited continuously during the entire swimming episode (Fig. 2*C*). Transiently recruited V2a

Significance

Spinal neural networks generate locomotion. An adjustment of the locomotion speed entails a precise order of recruitment of excitatory interneurons (e.g., V2a interneurons) within these networks. We show, using the adult zebrafish spinal cord, that the recruitment order of V2a interneurons is not topographic and does not conform to input resistance. The incremental recruitment of these interneurons is determined by scaling the excitatory drive with input resistance. We also show that locomotor networks are composed of multiple microcircuits recruited in a continuum. Thus, we provide insights into the recruitment mechanisms of spinal microcircuits that ensure optimal execution of locomotor movements.

Author contributions: J.A., R.M., and A.E.M. designed research; J.A. and R.M. performed research; J.A., R.M., and A.E.M. analyzed data; and J.A., R.M., and A.E.M. wrote the paper.

The authors declare no conflict of interest.

This article is a PNAS Direct Submission.

[1]To whom correspondence should be addressed. E-mail: Abdel.ElManira@ki.se.

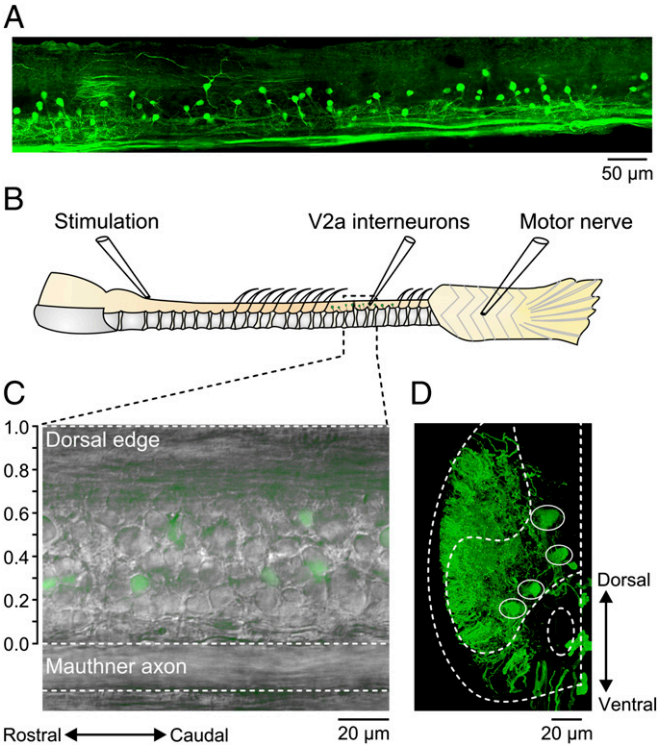

Fig. 1. Experimental setup and distribution of V2a interneurons. (*A*) Lateral view of a reconstructed spinal cord showing the distribution of V2a interneurons along the dorsoventral and rostrocaudal axis. (*B*) Schematic drawing of the in vitro brainstem/spinal cord preparation. (*C*) Overlay of DIC and fluorescence images showing V2a interneurons expressing GFP. The vertical scale axis shows how the soma position is measured using the normalized distance between the dorsal edge of the Mauthner axon and the dorsal edge of the spinal cord. (*D*) Transverse section of the spinal cord showing the dorsoventral and mediolateral distribution of V2a interneurons (circles). Dashed lines mark the spinal cord outline and the position of the Mauthner axon.

interneurons fired action potentials only at higher frequencies and displayed subthreshold locomotor-related membrane potential oscillations at low swimming frequencies (n = 20; Fig. 2*B*). Continuously recruited V2a interneurons fired bursts of action potentials throughout the swimming episode (n = 6; Fig. 2*C*). These results show that different V2a interneurons have different recruitment thresholds and display preferential firing patterns and membrane potential changes during swimming.

Incremental Recruitment of V2a Interneurons During Swimming. To determine if there are subsets of V2a interneurons that become recruited at different frequency thresholds, we assessed the change in the peak-to-trough amplitude of the locomotor-related membrane potential oscillations with increasing swimming frequencies. In nonrecruited V2a interneurons the amplitude of synaptic membrane potential oscillations covaried linearly with the swimming frequency (Fig. 2 *D* and *E*; blue). The slope of the change in oscillation amplitude varied considerably among the population of V2a interneurons (Fig. 2*E*). Nonrecruited V2a interneurons displayed a shallower change in the amplitude of membrane potential oscillations as a function of swimming frequency, and none of these interneurons was recruited at frequencies up to 10 Hz (Fig. 2*E*; blue). In transiently recruited V2a interneurons, the amplitude of subthreshold locomotor-related membrane potential oscillations always was linearly correlated with the swimming frequency (Fig. 2 *D* and *E*; filled red circles), and the mean slope of these oscillations was significantly ($P < 0.0001$) different from that of the nonrecruited V2a interneurons (Fig. 2*E*). In this set of V2a interneurons, a sudden increase in the amplitude of the oscillations at the threshold recruitment frequency brought them to firing (Fig. 2*D*; filled red circles). This set of V2a interneurons was incrementally recruited at swimming frequencies ranging from 3 to 5 Hz. In contrast, continuously recruited V2a interneurons were active at the onset of locomotor activity and displayed locomotor-related membrane potential oscillations that nearly always exceeded the firing threshold and remained relatively constant at all swimming frequencies (Fig. 2*D*; open red circles). Once V2a interneurons were recruited, the average number of action potentials did not depend on the locomotor frequency, because the spike frequency increased as the locomotor frequency increased (Fig. 2*F*). These results show that different subsets of V2a interneurons are recruited incrementally to cover swimming frequencies between 1 and 10 Hz, a range that represents 70% of the frequencies at which intact juvenile/adult zebrafish swim (37).

Recruitment Order of V2a Interneurons Is Not Topographically Organized. In embryonic and larval zebrafish, the order of recruitment of V2a interneurons correlated with their dorsoventral position in the spinal cord (15, 32, 36). This topographic organization of V2a interneuron recruitment is not maintained in juvenile/adult zebrafish. The somata of nonrecruited and recruited V2a interneurons (blue and red circles, respectively, in Fig. 3) were intermingled without any clear correlation between their position and order of recruitment during swimming (Fig. 3*A*). The motor column in juvenile/adult zebrafish extends both dorsoventrally and mediolaterally (22), whereas V2a interneurons were distributed diagonally from dorsomedial to ventrolateral in the ventral spinal cord (Figs. 1D and 3A). We projected the 2D location of each neuron onto a diagonal axis to define the relative position of V2a interneurons (Fig. 3*A*). None of the results described below were qualitatively different when the same data were plotted over the ventrodorsal or mediolateral axes separately as compared with the diagonal axis.

We next examined if the input resistance of V2a interneurons and the amplitude of locomotor-related membrane potential oscillations recorded at swimming frequencies of 4–5 Hz are topographically organized. Neither the input resistance (R^2 = 0.002; n = 46; Fig. 3*B*) nor the membrane oscillation amplitude (R^2 = 0.11; n = 48; Fig. 3*C*) was correlated with the position of V2a interneurons. In addition, there was no correlation between the minimum recruitment frequency of V2a interneurons and their relative position along the diagonal axis (R^2 = 0.03; n = 26; Fig. 3*D*). The differences in the amplitude of the membrane potential oscillations and the threshold frequency of V2a interneurons could reflect variations in their input resistance. However, we found no correlation between the input resistance of V2a interneurons and the peak-to-trough amplitude of the locomotor-related membrane potential oscillations (R^2 = 0.12; n = 46; Fig. 3*E*) or the minimum recruitment frequency (R^2 = 0.18; n = 24; Fig. 3*F*). The amplitude of the membrane potential oscillations at 4–5 Hz in the recruited V2a interneurons was a good predictor of recruitment, because it exceeded 5 mV in all the recruited interneurons (26 recruited V2a; Fig. 3 *C* and *E*), whereas it was lower than 5 mV in the majority of the nonrecruited V2a interneurons (20 of 22 nonrecruited V2a; Fig. 3 *C* and *E*). These results indicate that the recruitment of V2a interneurons is neither a reflection of their topographic organization nor a simple input-output transformation imposed by their input resistance.

Tuning the Recruitment Threshold by Scaling of Synaptic Inputs of V2a Interneurons. We next examined whether the amplitude of locomotor-related membrane potential oscillations and the recruitment threshold are determined by the amplitude of the synaptic drive these interneurons receive during swimming. We recorded excitatory and inhibitory currents underlying on-cycle excitation and mid-cycle inhibition from nonrecruited and recruited

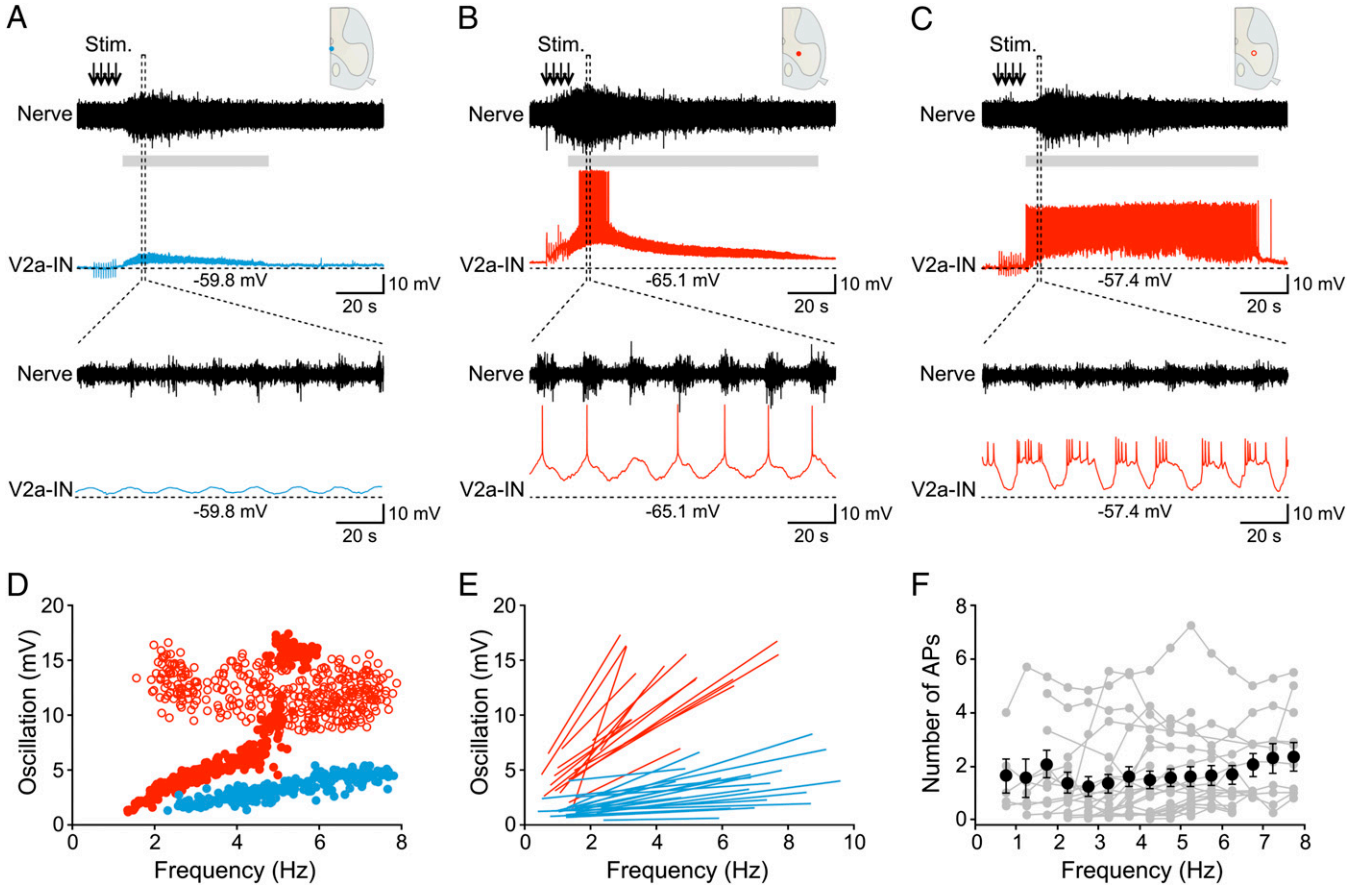

Fig. 2. Incremental recruitment of V2a interneurons with increased swimming frequency. (*A*) Recording from a V2a interneuron displaying only subthreshold locomotor-related membrane potential oscillations (blue) and a corresponding nerve recording (black). (*B*) Recording from a V2a interneuron transiently recruited during the swimming episode (red) and a corresponding nerve recording (black). (*C*) Recording from a V2a interneuron recruited continuously during the entire swimming episode (red) and a corresponding nerve recording (black). (*A–C Insets*) Position of the recorded interneurons in the spinal cord. Gray bars indicate the duration of the swimming episode. IN, interneuron. (*D*) Incremental increase in the peak-to-trough amplitude of the locomotor-driven membrane potential oscillations as a function of swimming frequency of the V2a interneurons in *A* (blue circles), *B* (filled red circles), and *C* (open red circles). (*E*) Slopes of the change in subthreshold locomotor-driven membrane potential oscillations from all nonrecruited (blue) and transiently recruited (red) V2a interneurons. Linear-fit lines cover the entire swimming episode for nonrecruited V2a interneurons. In transiently recruited V2a the linear fit lines cover all subthreshold locomotor cycles. (*F*) Plot showing the number of action potentials (APs) as a function of swimming frequency. Gray circles indicate individual neurons; black circles indicate averages from all neurons).

V2a interneurons (Fig. 4) by voltage-clamping neurons at the reversal potential of excitatory (0 mV) or inhibitory (−65 mV) currents. Results for transiently and continuously recruited neurons were not significantly different and thus were pooled in the following analysis. The amplitude of the excitatory inward currents showed a linear increase as a function of swimming frequency in both nonrecruited (R^2 = 0.49 ± 0.07; n = 13; Figs. 4A and 5A; mean amplitude = 11.4 ± 1.8 pA at 4–5 Hz swimming frequency; n = 13) and recruited V2a interneurons (R^2 = 0.51 ± 0.09; Figs. 4C and 5C; mean amplitude = 16.8 ± 1.7 pA at 4–5 Hz swimming frequency; n = 11). In contrast, the amplitude of the inhibitory outward current was not correlated with the swimming frequency (R^2 = 0.08 ± 0.02; n = 17) and remained relatively constant throughout the swimming episode in both nonrecruited (Figs. 4*B* and 5*B*; mean amplitude = 40.7 ± 3.9 pA at 4–5 Hz swimming frequency; n = 10) and recruited V2a interneurons (Figs. 4D and 5D; mean amplitude = 79.2 ± 30.0 pA at 4–5 Hz swimming frequency; n = 7). The correlation of the amplitude of the excitatory synaptic currents in V2a interneurons with the swimming frequency and the lack of correlation of the inhibitory currents suggests that the excitatory drive plays a more prominent role in setting the recruitment frequency threshold. We therefore focused our analysis on excitatory currents.

We found that the excitatory current amplitude showed a clear correlation with the relative position of V2a interneurons along the diagonal axis (R^2 = 0.43; Fig. 5*E*) and increased significantly with more ventral and lateral positions ($P < 0.001$). However, this apparent topographic organization of the strength of excitatory drive did not match the order of recruitment of V2a interneurons, indicating that the excitatory synaptic drive alone is insufficient to account for the recruitment threshold of V2a interneurons. This result also raises questions about how this topographically organized synaptic drive is transformed into a nontopographic recruitment pattern and how the synaptic currents are scaled to match the recruitment order of V2a interneurons.

To answer these questions, we calculated the change in voltage elicited by excitatory currents according to Ohm's law by multiplying excitatory synaptic currents by the input resistance of each neuron (Fig. 5*F*), and we compared that value with the measured locomotor-related amplitude of the membrane potential oscillation in the same interneuron (Fig. 5*G*). The calculated excitatory inputs indeed differentiated recruited from nonrecruited neurons, and the topographic order of the synaptic inputs was lost (Fig. 5*F*). The estimated synaptic depolarization always exceeded 5 mV in recruited V2a interneurons but did not reach 5 mV in the majority of the nonrecruited interneurons (Fig. 5*F*).

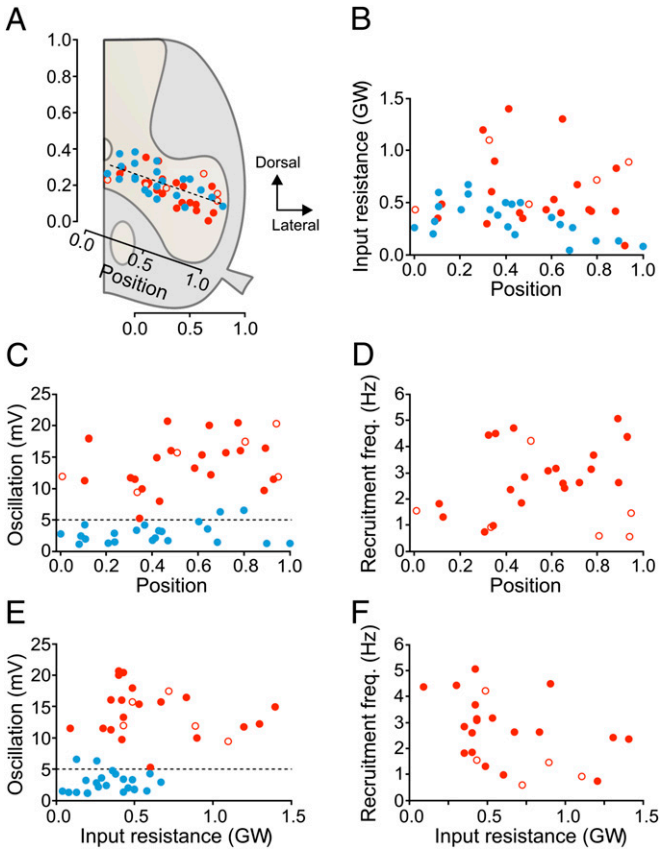

Fig. 3. The recruitment pattern of V2a interneurons is not topographically ordered. Blue circles indicate nonrecruited V2a interneurons; filled red circles indicate transiently recruited V2a interneurons; open red circles indicate continuously recruited V2a interneurons. (*A*) Lack of a topographic organization of recruited vs. nonrecruited V2a interneurons. (*B*) Plot of the input resistance of V2a interneurons as a function of the relative soma position (0: extreme dorsomedial; 1: extreme ventrolateral position within the population). (*C*) Plot of the average peak-to-trough amplitude of locomotor-related membrane potential oscillations (at 4–5 Hz swimming frequency) as a function of the relative soma position. Almost all the recruited V2a interneurons displayed locomotor-related membrane potential oscillations with amplitudes above 5 mV (dashed line). (*D*) Plot of the minimum recruitment frequency as a function of the relative soma position. (*E*) Plot of the average peak-to-trough amplitude of locomotor-related membrane potential oscillations (at 4–5 Hz swimming frequency) as a function of the input resistance of recruited and nonrecruited V2a interneurons. (*F*) Plot of the minimum recruitment frequency as a function of the input resistance.

Comparing the calculated excitatory inputs with the measured amplitude of the locomotor-related membrane potential oscillation confirmed that calculated inputs generally agreed with the actual amplitude of the membrane potential oscillation (R^2 = 0.33; n = 24; $P < 0.005$; Fig. 5*G*). Together these results show that the input resistance of the V2a interneurons transforms a topographically organized excitatory synaptic drive into nontopographic activity patterns and, as a consequence, shapes the recruitment pattern of V2a interneurons. Therefore, the recruitment threshold of the V2a interneurons is the result of the combined effect of their excitatory synaptic currents and input resistance, and neither of these factors alone is sufficient to predict the recruitment of these interneurons.

Temporal Relationship of Activity of V2a Interneurons and Motoneurons During Swimming. The results described above show that different V2a interneurons are recruited incrementally at different swimming frequencies, similar to the recruitment scheme of the different pools of motoneurons (22) but without an apparent topographic organization. V2a interneurons are considered one of the main sources for excitation of motoneurons, and it is conceivable that the recruited and nonrecruited V2a interneurons and motoneurons form microcircuits with some overlapping connectivity that are recruited at different swimming frequencies. It is possible that the activity of V2a interneurons and motoneurons in the recruited and nonrecruited circuits display their peak activity at distinct phases of the swimming cycle. We therefore examined the relative timing of the activity of V2a interneurons and motoneurons in relation to the locomotor bursts recorded in peripheral nerves using cross-correlations (Fig. 6). All V2a interneurons and motoneurons received phasic on-cycle excitation alternating with mid-cycle inhibition, and action potentials occurred at the peak of the depolarization in the recruited neurons (Fig. 6*A*). The average peak activity in the recruited motoneurons occurred at the midburst of the peripheral motor nerve but was preceded by that of the recruited V2a interneurons (Fig. 6 *A* and *B*). The peak depolarization of nonrecruited V2a interneurons and motoneurons occurred after the midburst of the motor nerve. These results show a clear temporal relationship between the locomotor-related membrane potential oscillations of recruited and nonrecruited V2a interneurons and motoneurons (Fig. 6 *A* and *B*).

The difference in the timing of the on-cycle excitation in recruited and nonrecruited neurons could result from the activation of voltage-dependent conductances or from a difference in the temporal pattern of the underlying synaptic currents. To test the latter possibility, we assessed the relationship between the excitatory current in recruited and nonrecruited neurons in reference to the motor nerve midburst during swimming. Indeed, the peak amplitude of the excitatory current occurred before the midburst in the motor nerve and preceded that of the recruited motoneurons (Fig. 6 *C* and *D*). Conversely, the peak amplitude of excitatory currents in nonrecruited V2a interneurons and motoneurons occurred after the midburst (Fig. 6 *C* and *D*). The inhibitory synaptic currents underlying mid-cycle inhibition, presumably arising from commissural V0 interneurons, occurred simultaneously in recruited V2a interneurons and motoneurons, and their timing preceded that of the nonrecruited neurons (Fig. 6 *E* and *F*).

Finally, we assessed the relationship between the timing of excitation and inhibition on a cell-by-cell basis by plotting the phase of inhibitory currents as a function of the corresponding excitatory currents. There was a significant correlation between the phase of the excitation and that of the inhibition in both V2a interneurons (R^2 = 0.55; n = 16; Fig. 6*G*) and motoneurons (R^2 = 0.67; n = 20; Fig. 6*H*). These results show that the timing of the excitatory and inhibitory synaptic currents of V2a interneurons and motoneurons covaries in a continuum that determines whether they are recruited during swimming.

Discussion

Pattern of Recruitment of V2a Interneurons. An optimal adjustment of the speed and force of locomotor movements requires a precise order of recruitment of the different neuronal components of the spinal networks, particularly those providing local excitation. However, the mechanisms setting the recruitment threshold of excitatory interneurons have remained unclear. Our findings in the juvenile/adult zebrafish spinal cord indicate that the incremental recruitment of V2a interneurons is defined by scaling a topographically organized excitatory synaptic drive with their input resistances. The recruitment order of these interneurons is not topographic and does not conform to variations in input resistance. Furthermore, the synaptic activity of recruited and nonrecruited V2a interneurons and motoneurons occurs in distinct phases of the locomotor cycle, suggesting that spinal locomotor networks are composed of multiple overlapping microcircuits

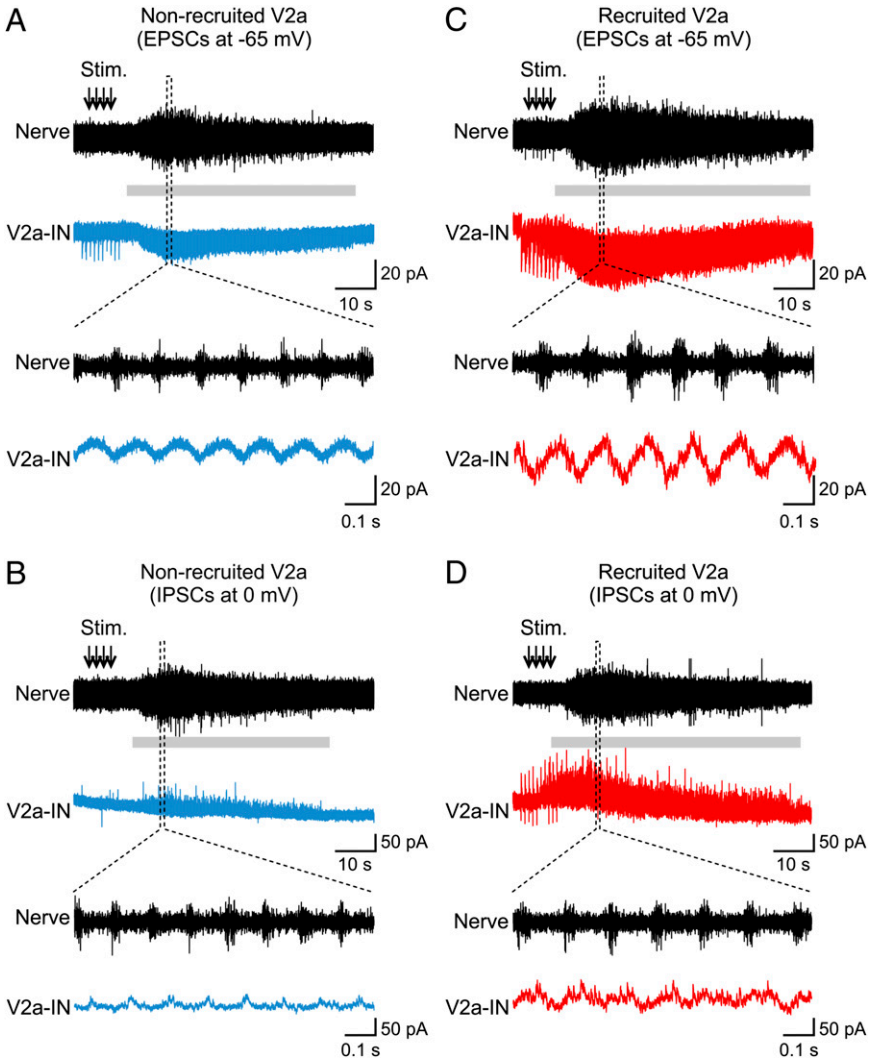

Fig. 4. On-cycle excitatory and mid-cycle inhibitory currents in V2a interneurons. Nerve recordings are shown in black and intracellular recordings in blue (for a nonrecruited V2a interneuron) or red (for a recruited V2a interneuron). Gray bars indicate the duration of the swimming episode. (*A*) On-cycle excitatory currents recorded in a nonrecruited V2a interneuron during a swimming episode. (*B*) Mid-cycle inhibitory currents recorded in the interneuron shown in *A* during a swimming episode. (*C*) On-cycle excitatory currents recorded in a recruited V2a interneuron during a swimming episode. (*D*) Mid-cycle inhibitory currents recorded in the interneuron shown in *C*.

encompassing subsets of interconnected V2a interneurons and motoneurons that are recruited in a continuum with increased swimming speeds.

Mechanisms Defining the Recruitment Threshold of V2a Interneurons. V2a interneurons represent a neuronal class of critical importance to the vertebrate locomotor network (1, 8, 12, 15, 25–35, 38). Their partial ablation in larval zebrafish decreases the excitability of the spinal networks and consequently increases the threshold for inducing swimming activity (30). Their pattern of activation during locomotion has been examined in both embryonic/larval zebrafish and newborn mice (32, 35). The pattern of activation of V2a interneurons both in newborn mice and embryonic/larval zebrafish is correlated in general to their input resistance (32). In embryonic and larval zebrafish the recruitment of V2a interneurons followed their topographic developmental order (15, 32, 36). Several differences emerge between the larval and the juvenile/adult zebrafish: (*i*) the topographic map becomes blurred, and the position of V2a interneurons no longer predicts their order of recruitment in the juvenile/adult stages; (*ii*) no shift in the recruited population of interneurons was apparent as the frequency increased from 1 to 10 Hz, although this shift may occur at higher swimming frequencies; and (*iii*) no correlation could be detected between the input resistance and the minimum recruitment frequency or the position of the V2a interneurons in the spinal cord.

We have shown previously that motoneurons in adult zebrafish are no longer recruited according to the principles of recruitment in larvae (22). It is clear that the locomotor pattern and frequency range display considerable differences in the embryonic/larval and the juvenile/adult stages, and these differences are associated with the lateral extension of the motor column and the development of slow motoneurons and muscle fibers that they innervate (39–41). Our results suggest that mechanisms underlying the recruitment of neurons in the spinal cord may undergo a refinement as the zebrafish develop toward adulthood. This refinement could be reflected in a reconfiguration of the organization of the swimming circuits to accommodate the changes in the swimming pattern and frequency range between early and adult developmental stages (10, 30, 36, 37, 42–45). It is not yet clear whether the scrambling of the topographic order of V2a interneuron recruitment mirrors only the displacement of

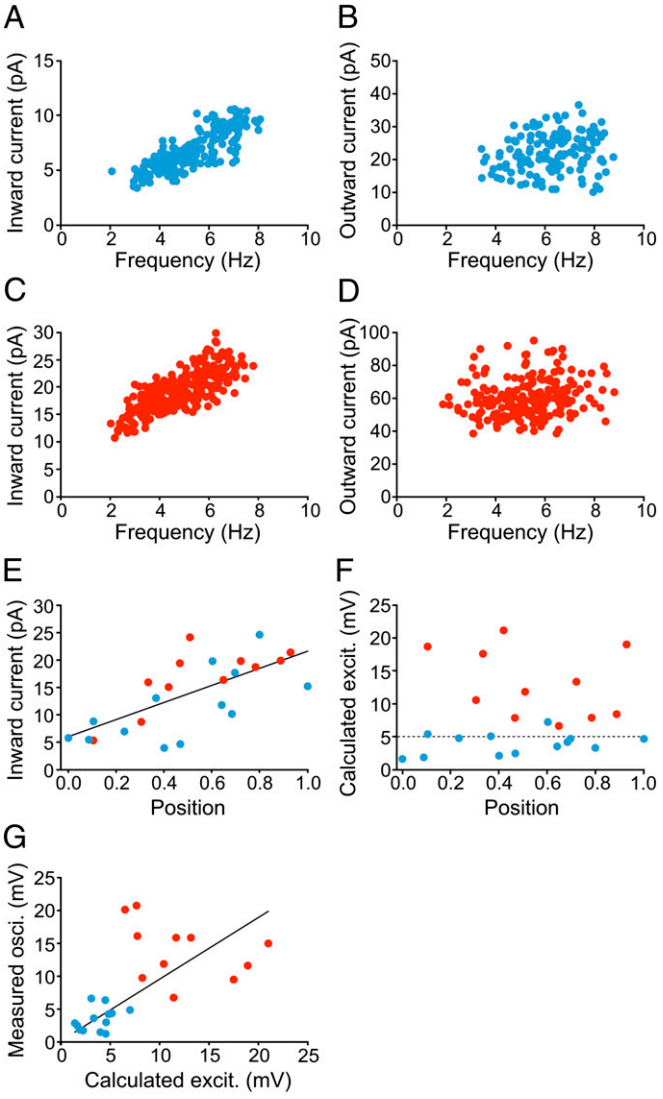

Fig. 5. Tuning the effect of synaptic currents encodes the order of recruitment of V2a interneurons. Blue circles indicate nonrecruited V2a interneurons; red circles indicate recruited V2a interneurons. (*A–D*) Graphs showing the change in the amplitude with swimming frequency of excitatory and inhibitory currents in a nonrecruited (blue circles) and a recruited (red circles) V2a interneuron. Data in these graphs are from the interneurons in Fig. 4. (*E*) Linear correlation (R^2 = 0.43) between the excitatory current amplitude and the relative soma position of V2a interneurons. (*F*) Graph showing the calculated excitatory inputs of V2a interneurons as a function of the relative soma position. The combination of the input resistance and the excitatory currents in each V2a interneuron predicts the 5-mV cut between nonrecruited and recruited V2a interneurons (dashed line). (*G*) The calculated excitation correlates well (R^2 = 0.33) with the measured locomotor-related membrane potential oscillations during swimming.

these interneurons, an additional tuning of their cellular and synaptic features, or both.

An important finding in this study is that the recruitment threshold of V2a interneurons is tuned by scaling the effect of excitatory synaptic drive by the input resistance. Interestingly, excitatory synaptic currents were organized topographically but failed to predict the order of recruitment of the V2a interneurons. The transformation of an orderly and topographically organized excitatory drive into a nontopographic pattern of recruitment seems to be achieved by a combined tuning of synaptic inputs and the input resistance of individual V2a interneurons. Thus, the computation of on-cycle excitatory currents and input resistance sets the recruitment threshold of the V2a interneurons.

Organization of the Locomotor Microcircuits in Zebrafish. Our results show that synaptic inputs of V2a interneurons and motoneurons with similar recruitment patterns display a similar temporal relationship. The timing of the inhibitory and excitatory synaptic inputs of V2a interneurons and motoneurons covaries in a continuum that determines whether they are recruited during swimming. We therefore suggest that the swimming network is composed of multiple overlapping microcircuits, which are recruited in a continuum as a function of increased swimming speed. These microcircuits are composed of topographically organized motoneurons and nontopographically organized V2a interneurons. It is likely that the neurons in each microcircuit are preferentially connected to each other, whereas connections between microcircuits are more sparse or weaker in strength.

The dorsoventral topographic organization of motoneurons seems to be maintained across different developmental stages in zebrafish with the addition of lateral motoneurons active during slow swimming in the adult stage (22, 23). This process is reminiscent of the development of the sensory-motor circuits in mice (46, 47). It is possible that motoneuron position is essential for appropriate connectivity of synaptic inputs and that it is likely to undergo minor positional adjustments. The connectivity between V2a interneurons and motoneurons with a similar recruitment threshold might need to be refined, because slow motoneurons start to differentiate only 2 wk posthatching (39). Our results provide insights into the organization of the swimming circuit and the mechanisms defining the recruitment of interneurons underlying excitation in zebrafish. The analysis of zebrafish locomotor networks at different developmental stages is beginning to shed light onto the principles governing the recruitment of different neuronal components that allow execution of movements with parameters appropriate for the behavioral context.

Experimental Procedures

In Vitro Spinal Cord Preparation. Zebrafish (*Danio rerio*) were raised and kept in a core facility at the Karolinska Institute according to established procedures (48). To enable selective targeting of V2a interneurons, we used a zebrafish line (Chx10:GFP) in which the expression of GFP was driven in V2a interneurons by the promoter of the transcription factor Alx (homolog of Chx10) (15). V2a interneurons have been described previously as excitatory circumferential descending interneurons (15, 49).

Zebrafish are considered juvenile 4 wk postfertilization and exhibit adult morphology with fully developed fins and pigmentation. Adult stages refer to breeding animals (~12 wk old). Animals used in this study were 6–10 wk old (18–25 mm body length) and are referred to as "juvenile/adult." All experimental protocols were approved by the Animal Research Ethical Committee, Stockholm. The preparation was performed as described previously (22, 37). Zebrafish were cold-anesthetized in frozen fish saline [134 mM NaCl, 2.9 mM KCl, 2.1 mM $CaCl_2$, 1.2 mM $MgCl_2$, 10 mM Hepes, and 10 mM glucose (pH 7.8), with NaOH 290 mOsm] and eviscerated. The skull was opened, and the brain was cut at the level of the midbrain. The epaxial musculature was removed up to the caudal end of the dorsal fin. The skin of the remaining tail musculature was removed gently. The vertebral arches were removed at the first two or three segments of the spinal cord to allow extracellular stimulation and at four or five segments rostral to the dorsal fin to expose the spinal cord and allow access with intracellular recording electrodes. The entire spinal cord and vertebral column together with the hindbrain and the caudal musculature were cut out. The preparation was transferred to the recording chamber, placed on the side, and fixed with Vaseline. During experiments, the preparations were perfused continuously with oxygenated fish saline at 20–22 °C, containing 10 μM D-tubocurarine to block neuromuscular junctions effectively and to abolish muscle twitches for the duration of the experiment.

GFP Staining. Fish were anesthetized with 0.1% MS-222 (Sigma-Aldrich) and intracardially perfused with 4% paraformaldehyde (vol/vol; Sigma-Aldrich) in PBS (0.01 M; pH 7.4). The tissues then were processed for whole-mount and section GFP immunostaining. The spinal cords for whole mounts were

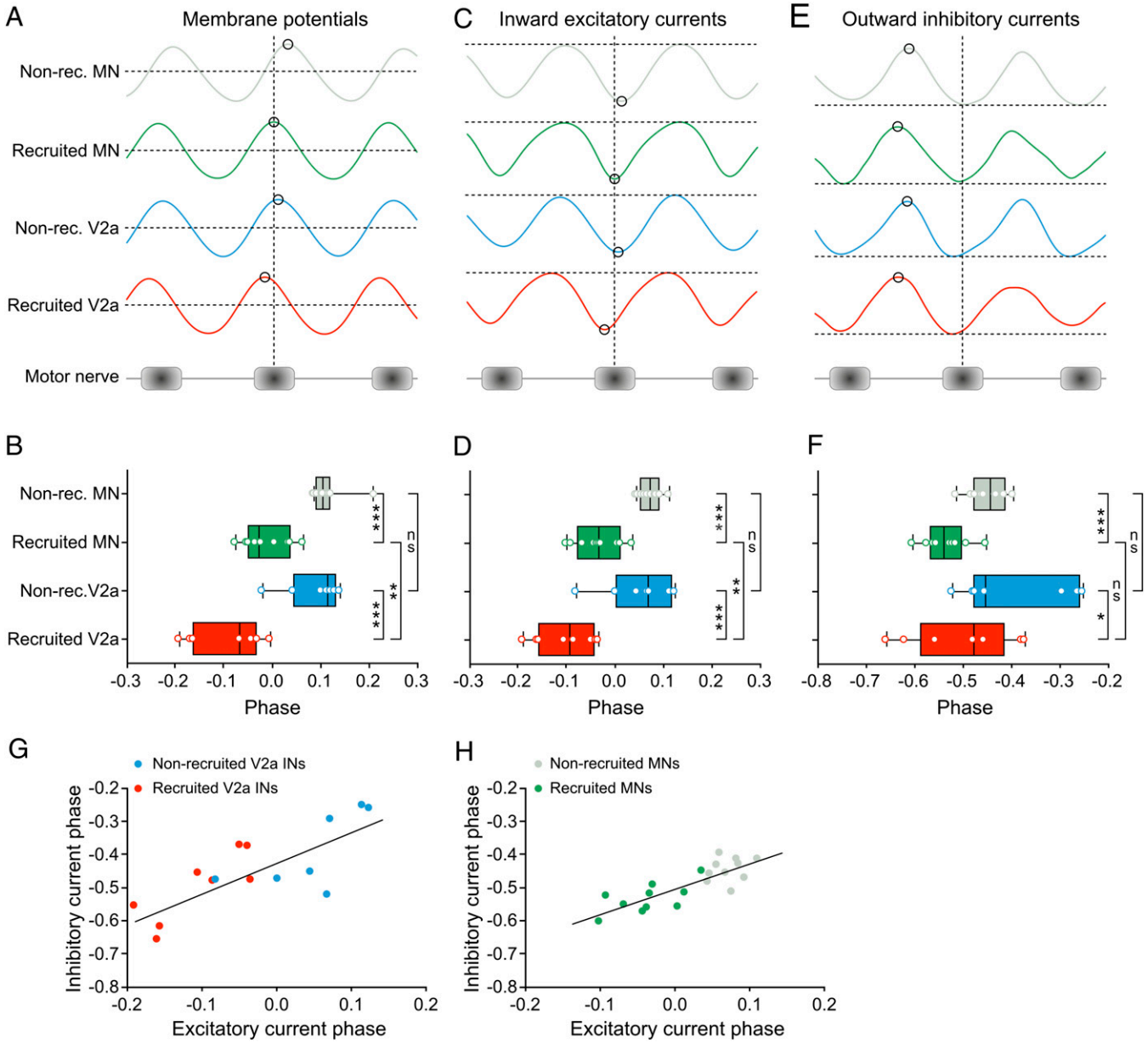

Fig. 6. Temporal relationship between V2a interneurons and motoneurons. (*A*) Cross-correlations showing the timing of the peak depolarization of the locomotor-related membrane potential oscillations (black circles) in recruited (red trace) and nonrecruited (blue trace) V2a interneurons and motoneurons (green traces) in relation to the activity in the peripheral motor nerve (schematically illustrated). (*B*) Box-and-whisker plot showing the average phase of the peak amplitude of locomotor-related membrane potential oscillations in the different neurons normalized to the cycle duration measured at the peripheral motor nerve. (*C*) Temporal relationship of the peak excitatory current (black circles) in recruited (red trace) and nonrecruited (blue trace) V2a interneurons and motoneurons (green traces) in relation to the activity of the peripheral motor nerve. (*D*) Box-and-whisker plot showing the average phase of the peak amplitude of the excitatory currents normalized to the cycle duration. (*E*) Temporal relationship of the peak inhibitory current (black circles) in recruited (red trace) and nonrecruited (blue trace) V2a interneurons and motoneurons (green traces) in relation to the activity of the peripheral motor nerve. (*F*) Box-and-whisker plot showing the average phase of the peak amplitude of the inhibitory current normalized to the cycle duration. The dashed lines in *A*, *C*, and *E* represent the baseline membrane potential or current. (*G* and *H*) The timing of excitatory and inhibitory currents covaries linearly in V2a interneurons (Ins) (R^2 = 0.55) (*G*) and motoneurons (MN) (R^2 = 0.67) (*H*).

placed in a cryoprotective solution (0.1 M phosphate-buffered 30% sucrose solution, wt/wt) for 2 h before being frozen. A cryostat was used to cut the tissues into 25-μm-thick coronal sections, which were collected on gelatin-coated slides. For GFP immunolabeling, sections and whole spinal cords were washed with PBS, and nonspecific protein-binding sites were blocked with 1% BSA (Sigma-Aldrich) and 0.3% Triton X-100 in PBS for 30 min at room temperature. Sections and whole-mount spinal cords then were incubated overnight at 4 °C in a moist chamber with rabbit anti-GFP (Abcam) diluted 1:650 in PBS. The tissues were rinsed in PBS three times for 5 min each washing and were incubated with Alexa Fluor-488 anti-rabbit IgG antibody (Molecular Probes) diluted 1:400 in PBS for 2 h at room temperature. The tissues then were rinsed in PBS and coverslipped with a glycerol-gelatin medium. Confocal images were obtained with a Zeiss LSM 510 laser-scanning confocal microscope.

Electrophysiology. Extracellular recording and stimulation electrodes were pulled from borosilicate glass (1-mm o.d., 0.87-mm i.d.; Harvard Apparatus), broken down to the desired tip diameter (15–25 μm), and fire-polished. Extracellular recordings were performed from the motor nerves running through the intermyotomal clefts at the tail, where the musculature was left

intact. A stimulation electrode was placed dorsally on the rostral spinal cord to elicit locomotor episodes by electrical stimulation (1 s at 30 Hz or 10 s at 1 Hz; pulse width, 1 ms; current amplitude, 0.3–1 mA). Extracellular signals were amplified (gain, 10,000) with a differential AC amplifier (A-M Systems) and filtered with low and high cutoff frequencies of 300 Hz and 1 kHz, respectively. Intracellular whole-cell recordings were performed from identified V2a interneurons rostral to the peripheral nerve recording. For intracellular recordings, electrodes were pulled from borosilicate glass (1.5-mm o.d., 0.87-mm i.d.; Hilgenberg) on a vertical puller (Narishige) and filled with intracellular solution [120 mM potassium gluconate, 5 mM KCl, 10 mM Hepes, 4 mM Mg_2ATP, 0.3 mM Na_4GTP, 10 mM sodium phosphocreatine (pH 7.4) with KOH, 275 mOsm], yielding resistances of 10–15 MΩ. GFP-labeled V2a cells were visualized with a fluorescent microscope (Axioskop FS Plus; Zeiss) equipped with IR-differential interference contrast (DIC) optics and a CCD camera with frame grabber (Hamamatsu) and then were targeted specifically. Intracellular patch-clamp electrodes were advanced into the exposed portion of the spinal cord through the meninges using a motorized micromanipulator (Luigs & Neumann) while applying constant positive pressure. Intracellular signals were amplified with a MultiClamp 700B intracellular amplifier (Axon Instruments) and low-pass filtered at 10 kHz. In current-clamp recordings, no bias current was injected. Only V2a interneurons that had stable membrane potentials at or below −48 mV, that fired action potentials to suprathreshold depolarizations, and that showed minimal changes in series resistance (<5%) were included in this study.

Determining Soma Size and Position. During the experiments, we captured images showing the outline of the soma as well as the dorsal edge of the spinal cord and the Mauthner axon. After the experiment, we analyzed the soma size and position using the measurement functions in ImageJ (http://rsb.info.nih.gov/ij). For the ventrodorsal soma position, we defined 1 as the dorsal edge of the spinal cord and zero as the dorsal edge of the Mauthner axon (Fig. 1*C*). The mediolateral position of the soma was measured during the experiment by focusing between the soma position, the lateral edge of the Mauthner axon, and the lateral surface of the spinal cord. For the mediolateral soma position, we defined zero as the lateral edge of the Mauthner axon and 1 as the lateral surface of the spinal cord. All positions and soma sizes were averaged from at least three individual measurements.

V2a interneurons were distributed along a diagonal line from dorsomedial to ventrolateral in the ventral spinal cord (Fig. 1*D*). We therefore projected the 2D location onto one diagonal axis to define the relative position of the V2a interneurons (Fig. 3*A*). To do so, we plotted the ventrodorsal soma positions over the mediolateral positions and fitted a linear regression function to the data ($R^2 = 0.39$; $y = -0.21$; $x = +0.26$). Soma positions in the 2D space then were projected onto the position on the linear fit that was closest to the original position. We then assigned the value zero to the most dorsomedial data point and the value 1 to the most ventrolateral soma position. The remaining data points were assigned values between zero and 1 depending on their position on the new diagonal axis (Fig. 3*A*).

Data Acquisition and Analysis. Data were digitized at 10 kHz (extracellular recordings) or 20 kHz (patch recordings) with a Digidata 1322A A/D converter (Axon Instruments) and acquired using pClamp software (version 10; Axon Instruments). Data analysis was performed in Matlab 2011a. The input resistance of neurons was calculated as the slope of a regression line to the linear region of the I–V curve (membrane potentials of −80 to −60 mV), which was obtained by injection of hyperpolarizing current pulses (duration, 1–2 s). The minimum recruitment frequency of V2a interneurons was defined as the slowest locomotor frequency of a swimming episode at which the neurons were firing action potentials. The minimum locomotor frequency obtained during swimming episodes varied between preparations. In some preparations the lowest frequency obtained was not lower than 4 Hz. To analyze the postsynaptic currents (PSCs), we voltage-clamped V2a interneurons close to the reversal potential of excitation (0 mV) or inhibition (−65 mV) (22, 42). We analyzed the peak-to-trough amplitude of the summed excitatory and inhibitory currents underlying the locomotor-driven membrane potential oscillations and not the individual PSCs. In all cases, the current traces were smoothed with a time constant of 0.01 s. In all neurons, the summed excitatory inward current occurred in phase with the ipsilateral motor nerve burst and was alternating with the summed inhibitory outward current (Fig. 4).

For the correlation analysis, intracellular traces were low-pass filtered (cutoff frequency 30 Hz), and a stretch of 10 s was cross-correlated with the corresponding rectified and smoothed (time constant, 0.01 s) extracellular nerve recordings. Phase shifts were measured as the time of the center peak of the cross-correlation to the origin (peak of the nerve recording autocorrelation) and normalized to the cycle period. Because the extracellular recording site was between 9 and 12 segments caudal to the respective intracellular recording site, we compensated the calculated phase shifts by subtracting the average phase shift per segment multiplied by the number of segments between the recording sites. The average phase shift per segment was obtained by calculating the phase shift per segment from 14 recruited motoneurons and the corresponding extracellular traces, assuming that motoneuron action potentials coincide with extracellular spikes of the same segment. Because action potentials could not be detected in voltage–clamp recordings, we were unable to distinguish between recruited and nonrecruited swimming cycles in these recordings. To overcome this problem, voltage-clamp recordings always were analyzed at the highest swimming frequencies ensuring analysis of spiking cycles for the transiently recruited interneurons.

All values are given as mean ± SEM. The significance of differences between the means in experimental groups and conditions was analyzed using the Student's two-tailed *t* test. Means were regarded as being statistically significant at $P < 0.05$.

ACKNOWLEDGMENTS. We thank Drs. R. Hill, S. Grillner, and O. Kiehn and members of our laboratory for comments and critical discussion of this manuscript and Drs. Joseph Fetcho and Shin-ichi Higashijima for providing the transgenic zebrafish line used in this study. This work was funded by grants from the Swedish Research Council, European Commission (FP7, Spinal Cord Repair), and Karolinska Institute. J.A. received a postdoctoral fellowship, AU 329/2-1, from the German Research Foundation.

1. Büschges A, Scholz H, El Manira A (2011) New moves in motor control. *Curr Biol* 21(13):R513–R524.
2. Fetcho JR, Higashijima S, McLean DL (2008) Zebrafish and motor control over the last decade. *Brain Res Brain Res Rev* 57(1):86–93.
3. Grillner S (2003) The motor infrastructure: From ion channels to neuronal networks. *Nat Rev Neurosci* 4(7):573–586.
4. Grillner S, Jessell TM (2009) Measured motion: Searching for simplicity in spinal locomotor networks. *Curr Opin Neurobiol* 19(6):572–586.
5. Kiehn O (2006) Locomotor circuits in the mammalian spinal cord. *Annu Rev Neurosci* 29:279–306.
6. Roberts A, Li WC, Soffe SR (2010) How neurons generate behavior in a hatchling amphibian tadpole: An outline. *Front Behav Neurosci* 4:16.
7. Rossignol S, Dubuc R, Gossard JP (2006) Dynamic sensorimotor interactions in locomotion. *Physiol Rev* 86(1):89–154.
8. Al-Mosawie A, Wilson JM, Brownstone RM (2007) Heterogeneity of V2-derived interneurons in the adult mouse spinal cord. *Eur J Neurosci* 26(11):3003–3015.
9. Dasen JS, Jessell TM (2009) Hox networks and the origins of motor neuron diversity. *Curr Top Dev Biol* 88:169–200.
10. Drapeau P, et al. (2002) Development of the locomotor network in zebrafish. *Prog Neurobiol* 68(2):85–111.
11. Fetcho JR, McLean DL (2010) Some principles of organization of spinal neurons underlying locomotion in zebrafish and their implications. *Ann N Y Acad Sci* 1198:94–104.
12. Goulding M (2009) Circuits controlling vertebrate locomotion: Moving in a new direction. *Nat Rev Neurosci* 10(7):507–518.
13. Jessell TM (2000) Neuronal specification in the spinal cord: Inductive signals and transcriptional codes. *Nat Rev Genet* 1(1):20–29.
14. Kiehn O (2011) Development and functional organization of spinal locomotor circuits. *Curr Opin Neurobiol* 21(1):100–109.
15. Kimura Y, Okamura Y, Higashijima S (2006) alx, a zebrafish homolog of Chx10, marks ipsilateral descending excitatory interneurons that participate in the regulation of spinal locomotor circuits. *J Neurosci* 26(21):5684–5697.
16. Kimura Y, Satou C, Higashijima S (2008) V2a and V2b neurons are generated by the final divisions of pair-producing progenitors in the zebrafish spinal cord. *Development* 135(18):3001–3005.
17. Ladle DR, Pecho-Vrieseling E, Arber S (2007) Assembly of motor circuits in the spinal cord: Driven to function by genetic and experience-dependent mechanisms. *Neuron* 56(2):270–283.
18. Lewis KE, Eisen JS (2003) From cells to circuits: Development of the zebrafish spinal cord. *Prog Neurobiol* 69(6):419–449.
19. Satou C, et al. (2009) Functional role of a specialized class of spinal commissural inhibitory neurons during fast escapes in zebrafish. *J Neurosci* 29(21):6780–6793.
20. Satou C, Kimura Y, Higashijima S (2012) Generation of multiple classes of V0 neurons in zebrafish spinal cord: Progenitor heterogeneity and temporal control of neuronal diversity. *J Neurosci* 32(5):1771–1783.
21. Tripodi M, Arber S (2012) Regulation of motor circuit assembly by spatial and temporal mechanisms. *Curr Opin Neurobiol* 22(4):615–623.
22. Gabriel JP, et al. (2011) Principles governing recruitment of motoneurons during swimming in zebrafish. *Nat Neurosci* 14(1):93–99.

23. McLean DL, Fan J, Higashijima S, Hale ME, Fetcho JR (2007) A topographic map of recruitment in spinal cord. *Nature* 446(7131):71–75.
24. Mendell LM (2005) The size principle: A rule describing the recruitment of motoneurons. *J Neurophysiol* 93(6):3024–3026.
25. Buchanan JT, Grillner S (1987) Newly identified 'glutamate interneurons' and their role in locomotion in the lamprey spinal cord. *Science* 236(4799):312–314.
26. Crone SA, et al. (2008) Genetic ablation of V2a ipsilateral interneurons disrupts left-right locomotor coordination in mammalian spinal cord. *Neuron* 60(1):70–83.
27. Crone SA, Zhong G, Harris-Warrick R, Sharma K (2009) In mice lacking V2a interneurons, gait depends on speed of locomotion. *J Neurosci* 29(21):7098–7109.
28. Dale N, Roberts A (1985) Dual-component amino-acid-mediated synaptic potentials: Excitatory drive for swimming in Xenopus embryos. *J Physiol* 363:35–59.
29. Dougherty KJ, Kiehn O (2010) Firing and cellular properties of V2a interneurons in the rodent spinal cord. *J Neurosci* 30(1):24–37.
30. Eklöf-Ljunggren E, et al. (2012) Origin of excitation underlying locomotion in the spinal circuit of zebrafish. *Proc Natl Acad Sci USA* 109(14):5511–5516.
31. Lundfald L, et al. (2007) Phenotype of V2-derived interneurons and their relationship to the axon guidance molecule EphA4 in the developing mouse spinal cord. *Eur J Neurosci* 26(11):2989–3002.
32. McLean DL, Masino MA, Koh IY, Lindquist WB, Fetcho JR (2008) Continuous shifts in the active set of spinal interneurons during changes in locomotor speed. *Nat Neurosci* 11(12):1419–1429.
33. Roberts A, Li WC, Soffe SR, Wolf E (2008) Origin of excitatory drive to a spinal locomotor network. *Brain Res Brain Res Rev* 57(1):22–28.
34. Zhong G, et al. (2010) Electrophysiological characterization of V2a interneurons and their locomotor-related activity in the neonatal mouse spinal cord. *J Neurosci* 30(1):170–182.
35. Zhong G, Sharma K, Harris-Warrick RM (2011) Frequency-dependent recruitment of V2a interneurons during fictive locomotion in the mouse spinal cord. *Nat Commun* 2:274.
36. McLean DL, Fetcho JR (2009) Spinal interneurons differentiate sequentially from those driving the fastest swimming movements in larval zebrafish to those driving the slowest ones. *J Neurosci* 29(43):13566–13577.
37. Kyriakatos A, et al. (2011) Initiation of locomotion in adult zebrafish. *J Neurosci* 31 (23):8422–8431.
38. Li WC, Moult PR (2012) The control of locomotor frequency by excitation and inhibition. *J Neurosci* 32(18):6220–6230.
39. van Raamsdonk W, Mos W, Smit-Onel MJ, van der Laarse WJ, Fehres R (1983) The development of the spinal motor column in relation to the myotomal muscle fibers in the zebrafish (Brachydanio rerio). I. Posthatching development. *Anat Embryol (Berl)* 167(1):125–139.
40. van Raamsdonk W, Pool CW, te Kronnie G (1978) Differentiation of muscle fiber types in the teleost Brachydanio rerio. *Anat Embryol (Berl)* 153(2):137–155.
41. van Raamsdonk W, van't Veer L, Veeken K, Heyting C, Pool CW (1982) Differentiation of muscle fiber types in the teleost Brachydanio rerio, the zebrafish. Posthatching development. *Anat Embryol (Berl)* 164(1):51–62.
42. Gabriel JP, et al. (2009) Serotonergic modulation of locomotion in zebrafish: Endogenous release and synaptic mechanisms. *J Neurosci* 29(33):10387–10395.
43. Gabriel JP, et al. (2008) Locomotor pattern in the adult zebrafish spinal cord in vitro. *J Neurophysiol* 99(1):37–48.
44. Masino MA, Fetcho JR (2005) Fictive swimming motor patterns in wild type and mutant larval zebrafish. *J Neurophysiol* 93(6):3177–3188.
45. McDearmid JR, Drapeau P (2006) Rhythmic motor activity evoked by NMDA in the spinal zebrafish larva. *J Neurophysiol* 95(1):401–417.
46. Jessell TM, Sürmeli G, Kelly JS (2011) Motor neurons and the sense of place. *Neuron* 72(3):419–424.
47. Sürmeli G, Akay T, Ippolito GC, Tucker PW, Jessell TM (2011) Patterns of spinal sensory-motor connectivity prescribed by a dorsoventral positional template. *Cell* 147(3):653–665.
48. Westerfield M (2000) *The Zebrafish Book. A guide for the Laboratory Use of the Zebrafish (*Danio rerio*)* (Univ of Oregon Press, Eugene, OR) 4th Ed.
49. Higashijima S, Schaefer M, Fetcho JR (2004) Neurotransmitter properties of spinal interneurons in embryonic and larval zebrafish. *J Comp Neurol* 480(1):19–37.